Elsevier Editorial System(tm) for Applied Surface Science
Manuscript Draft

Manuscript Number:

Title: Preparation and characterization of low-crystallized hydroxyapatite nanoporous plates and granules

Article Type: Research Paper

Keywords: hydroxyapatite; nanoparticle; assembly; transparency; nanopore; protein adsorption

Corresponding Author: Dr. Masahiro Okada, Ph.D.

Corresponding Author's Institution: Osaka Dental University

First Author: Mayo Uehira, DDS

Order of Authors: Mayo Uehira, DDS; Masahiro Okada, Ph.D.; Shoji Takeda, Ph.D.; Naoyuki Matsumoto, DDS

Manuscript Region of Origin: JAPAN

Suggested Reviewers: Thomas J. Webster Ph.D
Professor, Division of Engineering, , Brown University
thomas_webster@brown.edu
He is a speciallist of nanostructured hydroxyapatite.

Ayako Oyane Ph.D
National Institute of Advanced Industrial Science and Technology
a-oyane@aist.go.jp
She is a specialist of hydroxyapatite/protein composites.

Ramin Rohanizadeh Ph.D
Professor, Advanced Drug Delivery Group, Faculty of Pharmacy, University of Sydney
ramin.rohanizadeh@sydney.edu.au
He is a specialist of protein adsorption onto the surface of calcium phosphate biomaterials.

Research highlights (maximum 85 characters, including spaces, per bullet point)

► Nanoparticle-assembled hydroxyapatite plates and granules were fabricated.
► They had nanosized open pores and the size of nanopores could be controlled.
► Various liquids and proteins could be infiltrated inside the nanopores.
► This method requires no pore generation agents such as micelles and porogens.

Preparation and characterization of low-crystallized hydroxyapatite nanoporous plates and granules

Mayo Uehira[1,*], Masahiro Okada[2,*], Shoji Takeda[2], Naoyuki Matsumoto[1]

[1]Graduate School of Dentistry, Department of Orthodontics, Osaka Dental University, 8-1 Kuzuha-Hanazono, Hirakata, Osaka 573-1121, Japan

[2]Department of Biomaterials, Osaka Dental University, 8-1 Kuzuha-Hanazono, Hirakata, Osaka 573-1121, Japan

*Corresponding authors:

M. Uehira: uehira-m@cc.osaka-dent.ac.jp (Tel: +81-72-864-3078)

M. Okada: okada-m@cc.osaka-dent.ac.jp (Tel: +81-72-864-3111)

Abstract (up to 200 words)

We examined the conditions for preparing nanoporous hydroxyapatite (HAp) plates and granules by assembling low-crystallinity HAp nanoparticles without template/binder molecules or high-temperature/pressure treatments. We first prepared HAp nanoparticles with different particle sizes and then the nanoporous plate or granule was prepared by drying an aqueous dispersion of HAp nanoparticles on an oil substrate. The hydrophobic oil substrate was preferable to prevent crack formation in HAp plates. The size of the HAp plate could be controlled by the concentration of HAp dispersion, and millimeter-sized granules were obtained by drying a small volume of HAp dispersion on/in the oil substrate. The nanoparticle-assembled HAp had nanosized pores, and the pore size could be changed by adjusting the size of the HAp nanoparticles used. It was found that both hydrophilic and hydrophobic liquids could infiltrate inside the nanopores. The nanoporous HAp granules also could adsorb and release proteins, and the protein adsorption and release delayed in the presence of the nanopores.

Keywords:

hydroxyapatite; nanoparticle; assembly; transparency; nanopore; protein adsorption

1. Introduction

Hydroxyapatite (HAp) is recognized as a major inorganic component of human hard tissues, and synthetic HAp exhibits excellent cell adhesion [1] because of favorable adsorption capacity of the HAp surface for bioactive substances such as cell-adhesive proteins [2]. Therefore, HAp and its composites with polymers or metals have been widely used in orthopedic and dental applications [3, 4]. Other important applications of HAp include their use as cell culture substrates to study cell behavior [5, 6] and supports for drug delivery [7].

Recently, nanosized structures of HAp ceramics have attracted interest because of their improved bioactivity compared with conventional HAp ceramics [8–12]. For example, Webster and coworkers [8, 9] showed an enhanced osteoclast-like cell adhesion and function on HAp ceramic surfaces with nanometer-sized surface topography. Sun *et al.* [10] reported that nanophase HAp can more effectively promote the proliferation and osteogenic differentiation of periodontal ligament cells compared with dense HAp.

In addition, nanoporous (or mesoporous) HAp ceramics have also been developed as supports for drugs and proteins. For example, Yao *et al.* [13] prepared HAp nanoparticles with channels approximately 3 nm in diameter by precipitating HAp onto rod-like micelles of cationic surfactants (cetyltrimethylammonium bromide, CTAB) in an aqueous medium. Ye *et al.* [14] reported micelle-templated synthesis of HAp hollow nanoparticles or nanotubes (outer diameter, <35 nm; inner diameter, 13 nm; length, 50–250 nm) with nonionic surfactants ($EO_{20}PO_{70}EO_{20}$; EO = ethylene oxide; PO = propylene oxide). Raksujarit *et al.* [15] recently reported the fabrication of nanoporous HAp ceramics using poly(vinyl alcohol) as a pore former. Thus, surfactant molecules, which may cause

allergy-like reactions and cytotoxicity [16], are generally required to fabricate nanoporous structures in HAp ceramics.

In our previous study [17], we preliminarily prepared nanoparticle-assembled plates, which consist of low-crystallinity HAp, by drying a HAp aqueous dispersion on an oil (flowable) substrate without template/binder molecules or high-temperature/pressure treatments. The nanoparticle-assembled HAp was relatively transparent and contained nanopores, which is significantly different from conventional transparent HAp sintered dense ceramics [18–21].

The objective of this study is to clarity the effects of preparation parameters (the type of oil substrate, the volume/concentration of HAp dispersion, and the HAp particle size) on the morphological change of nanoparticle-assembled HAp. Here particular attention is given to the surface morphology, the pore size (and its distribution), the transparency and the crystallinity using scanning electron microscopy (SEM), mercury intrusion porosimetry, ultraviolet-visible (UV-Vis) spectrophotometry and X-ray diffraction (XRD), respectively. The infiltration of various liquids and the adsorption/release of proteins were also investigated to evaluate the effectiveness of the nanopores inside the nanoparticle-assemble HAp.

2. Experimental

2.1. Materials

Unless otherwise stated, all materials were guaranteed reagent grade and used as received from Wako Pure Chemical Industries, Ltd., Osaka, Japan. Milli-Q water (Millipore Corp., Bedford, MA) with a specific resistance of 18.2×10^6 Ω·cm was used.

2.2. HAp nanoparticles

The conditions for preparing HAp nanoparticles are listed in Table 1. Briefly, an aqueous solution of calcium salts (42 mM, 800 mL), whose pH was adjusted by addition of 28% ammonia solution, was poured into a 1-L reactor equipped with an inlet for nitrogen and a magnetic stirrer. After the temperature in the reactor had been equilibrated to a predetermined temperature (20˚C or 60˚C), an aqueous solution of phosphate salts (100 mM, 200 mL) was added into the reactor, and the resultant mixture was stirred for another 24 h at the temperature. The resulting product was then centrifugally washed until the pH of the solution became neutral, and then redispersed in water.

The nanoparticles washed were observed using an S-4800 SEM (Hitachi High Technologies Corp., Tokyo, Japan) operated at 5 kV, after the samples were dried on an aluminum stub at room temperature and sputter-coated with Pt–Pd to minimize sample-charging problems. The number-averaged particle size (N = 50) was determined from SEM photographs.

To identify the crystal phases of the samples, powder XRD measurements were performed using an XRD-6100 (Shimadzu Corp., Kyoto, Japan) equipped with a CuKα radiation source, after the dried samples were ground using a mortar and pestle.

<Table 1>

2.3. HAp-nanoparticle-assembled plates and granules

A typical procedure for preparing the platesis as follows. Pentadecane, 1-dodecanol or

their mixture was used as a liquid substrate; it was spread on a polytetrafluoroethylene (PTFE) dish (inner diameter, 10 cm) at room temperature. After the HAp dispersion (2.0 wt.%) was degassed under reduced pressure at room temperature for approximately 3 min, 5 mL of the dispersion was gently cast onto the center of the liquid substrate, and the dish was subsequently placed in a thermostat drying oven at 60°C for 12 h. The transparent plate obtained after drying the dispersion was immersed three times in pure ethanol to remove the oil substrate, and then dried at room temperature.

The granules were prepared in the same manner except for the volumes of HAp dispersion (50 μL) and pentadecane (10 μL) in a 96-well PTFE multiplate with round bottom (the inner diameter of each well, 6.5 mm).

The surfaces of the samples were observed using an S-4800 SEM operated at 5 kV, after the samples were fixed onto an aluminum stub and sputter-coated with Pt–Pd.

The pore-size distributions, porosities and specific surface areas were determined using mercury intrusion porosimetry (AutoPore IV 9520; Micromeritics Instrument Corp., Norcross, GA), after the samples were dried under vacuum at 60°C for 24 h.

The solid-state densities of the samples were determined using helium pycnometry (AccuPyc 1330; Micromeritics Instrument Corp., Norcross, GA), after the samples were ground using a mortar and pestle and dried under vacuum at 60°C for 24 h.

The transmittance of visible light (λ, 400–700 nm) was recorded with a UV-Vis spectrophotometer (V-550; JASCO Corp., Tokyo, Japan) to evaluate the visible light transparency.

2.4. Protein adsorption and release

The HAp granules were examined as a protein carrier. As model proteins, albumin (BSA: Bovine serum albumin, Thermo Fisher Scientific Inc., Rockford, IL) and Cytochrome C (Cyt-c; Wako Pure Chemical Industries, Ltd.) were used in this study. Each protein was dissolved in a Dulbecco's phosphate buffered saline (PBS: without Ca and Mg; pH 7.4; Nacalai Tesque, Inc., Kyoto, Japan) and the initial protein concentration was set to 200 μg/mL. For the protein adsorption, 10 granules (total, 10 mg) were immersed in each protein solution (0.5 mL) in a 48-well multiplate at room temperature for 10 days. The amount of protein adsorbed was calculated from the protein concentration in a supernatant (0.1 mL). For the protein release, the 10 granules after the protein adsorption for 10 days were rinsed with PBS once and then placed in a fresh PBS (0.5 mL) at 37˚C. The percentage of the protein released against the total amount of the protein in each sample was calculated from the protein concentration in a supernatant (0.1 mL). The medium was replaced with a fresh PBS once a three time withdrawing the supernatant.

The above tests were repeated three times (N=3), and the protein concentration in each supernatant was determined using a Pierce's BCA Protein Assay Reagent Kit (Thermo Fisher Scientific Inc.) following the manufacture’s standard protocol, and the absorbance at 562 nm was measured three times with a microplate reader (SpectraMax M5; Molecular Devices, LLC., Sunnyvale, CA). DATA resulting from the tests were presented as means ± standard deviations for the mean.

3. Results and Discussion

3.1. Preparation of HAp nanoparticles

We prepared four types of HAp nanoparticles with different particle sizes by the wet

chemical processes. In order to obtain the particles with different sizes, the sources of calcium/phosphate salts, temperature and feed rate were varied as shown in Table 1 (see also Supplementary Fig. S1 for SEM photographs). In the case of $(CH_3COO)_2Ca$ as a calcium source, spherical particles with smallest particle size (31 nm) were obtained, which should be due to the inhibition of crystal growth by adsorbing the CH_3COO- ions onto a HAp surface [22,23]. In the case of $Ca(NO_3)_2$ as a calcium source, 46-nm sized spherical particles were obtained at 20˚C, and slightly elongated (73-nm sized) and polydispersed particles were obtained at an elevated temperature (60˚C) under a fast feed rate (within 5 sec) of phosphate salt solution. Larger rod-shaped (320 nm in length) and polydispersed particles were obtained under a slow feed rate (20 mL/h). Hereafter, the particles used were abbreviated as HAp-31, HAp-46, HAp-73 and HAp-320 (see Table 1), where each numerical value indicates the particle size (or length).

The XRD measurement for each nanoparticle showed a broad pattern of HAp (JCPDS PDF No. 9-732), and no other calcium phosphate phases could be detected (Fig. 1). The broad pattern of the samples suggests the formation of low-crystallinity HAp, which shows higher solubility compared with well-crystallized HAp [24]. In the case of larger particles prepared under higher temperature, several peaks became slightly distinct, which indicates the increase in the crystallinity.

<Fig. 1>

3.2. Preparation of HAp-nanoparticle-assembled plates and granules

In this study, the HAp-nanoparticle-assembled plate (or granule) was prepared by

drying the HAp aqueous dispersion on an oil (flowable) substrate [17] because simple casting on a solid hydrophobic PTFE substrate led to the formation of cracks in the plate. Thick films prepared from colloidal dispersions, such as latex [25,26], wet clay [27] and ceramic slips [28,29], are also known to crack while drying on rigid substrates due to the following mechanism. Colloidal particles accumulate at the surface (water/air and water/substrate interfaces) of a dispersion droplet and thus a low-fluidity gel forms in the circumference of the dispersion droplet with water evaporation. Further water evaporation compels to shrinkage of the gel at the water/air interface, which leads to large stresses and causes crack formation. The rigid substrate imposes a constraint of the gel at the water/substrate interface, which prevents complete relaxation of the stress [28]. By drying on an oil substrate, the stresses can be relaxed because the substrate is flowable, and the interfacial tension between the water/oil substrate is expected to aid the shrinkage of the aqueous dispersion during the drying.

In the previous study, we used a neutral paraffinic oil $\{(CH_2)_n,\ 20 \leq n \leq 40\}$ as a oil substrate. In this study, first, the influence of the oil type was examined by drying HAp-46 dispersions (2.0 wt.%; 5 mL) on hydrophobic oil (pentadecane) and hydrophilic oil (1-dodecanol) substrates (Fig. 2). In the case of pure pentadecane, the spreading area of HAp dispersion on the oil substrate before drying was the smallest (*i.e.*, the interfacial tension between HAp dispersion and pure pentadecane was the largest) and the crack formation could be prevented after drying (see also Fig. 3b). The addition of 1-dodecanol in pentadecane induced the spreading of the HAp dispersion (and hence the spreading of the HAp plate after drying) on the oil substrate. Cracks were formed after drying on the substrate containing above 40 vol.% of 1-dodecanol. These results support that the interfacial tension

between the aqueous medium and the oil substrate is a key factor to prevent the crack formation in nanoparticle-assembled plates.

<Fig. 2>

Next, the influence of the particle concentration of HAp dispersion was examined by drying HAp-46 dispersion (5 mL) on pure pentadecane substrates (see Supplementary Fig. S2). The size (diameter) and thickness of nanoparticle-assembled HAp plate decreased with a decrease in the concentration of the HAp dispersion casted on the oil substrate. The total volume of HAp dispersion casted on the oil substrate also influenced on the plate size. An extremely reduced volume of HAp dispersion lead to the formation of granules rather than plates. Actually, after drying 50 μL of HAp dispersion (2.0 wt.%) on/in a pentadecane substrate, granules with around 1.5 mm diameters were obtained (see Figs. 3i–l).

Finally, the influence of the particle size was examined by drying HAp dispersions (2.0 wt.%; 5 mL) on pure pentadecane substrates (Fig. 3). Before drying, the spreading area of the dispersion was almost constant (diameter, around 4 cm) regardless of the particle size. After drying, although the HAp-31, HAp-46 and HAp-73 plates had almost the same diameter (approximately 1.0 cm), the HAp-320 plate had larger diameter (approximately 1.2 cm; Fig. 3d) than other plates, which suggests that the shrinkage of the dispersion droplet was prevented and that the particle coordination number [30] decreased in the case of larger (rod-shaped) particles.

<Fig. 3>

3.3. Transparency of HAp-nanoparticle-assembled plates

The HAp-31 or HAp-46 plate prepared by casting on a pentadecane substrate was remarkably transparent in the oil (see Figs. 3a and 3b), which should be due to the small particle/pore size [31] and due to infiltration of pentadecane, whose refraction index is greater than that of air, inside the pores. Although the transparency of the HAp-31 or HAp-46 plates decreased after removal of pentadecane (Figs. 3e–f and 4a), the dried plate returned to high transparency after the plate was re-immersed in oil substrate (Fig. 4b). On the other hand, the HAp-320 plate was almost opaque regardless of the infiltration of pentadecane, which suggests the plate had large particle/pore size.

In order to observe viable cells (or living tissue through skin tissue) with an optical microscope in situ, a cell culture substrate (or a percutaneous device [1]) having high transparency is preferred. Although various processes have been developed to prepare transparent HAp sintered bodies [1, 18–21], all of them involve costly procedures including long-term or high-temperature, high-pressure, or high-voltage treatment. In addition, the composition and structure of the sintered HAp have limited variety, and are largely different from natural bone apatite [1, 32]. High-temperature synthesis (sintering) causes high crystallinity, low specific surface area, and poor reactivity, whereas the transparent HAp plates prepared here were low crystallinity like biological apatite with high surface reactivity. Hong et al. demonstrated that osteoblasts on low-crystallinity HAp thin film exhibited a high cellular activity such as adhesion, proliferation and differentiation with the formation of calcified matrix [33].

<Fig. 4>

3.4. Morphology of HAp-nanoparticle-assembled plates

The SEM observations revealed that the surfaces of HAp-nanoparticle-assembled plates were relatively flat in low-magnified images (Fig. 5), which might be due to the interfacial tension between the aqueous medium and the oil substrate during drying. In high-magnified images (insets of Fig. 5), nanosized pores were observed between the nanoparticles. Note that the nanosized pores (i.e., nanosized surface roughness) would affect various cell activities [8–12].

<Fig. 5>

Mercury intrusion porosimetry was performed to quantitatively determine the nanopores. Figure 6 shows pore-size distributions of the samples prepared from HAp nanoparticles with different particle sizes (see also Supplementary Table S1). The mean pore size increased in an increase in the particle size of HAp. The porosities of the plates were ranging from 54 to 80%, and increased with an increase in the particles size. In the case of a monodispersed spherical particle assembly with a hexagonal close-packed structure, the theoretical porosity (due to the gap between the particles) is 26%, and the porosity decreases with an increase in polydispersity of the particles. Thus, the large porosity (54–76%) of the sample indicates the presence of gaps between randomly packed (aggregated) particles.

<Fig. 6>

Judging from data obtained from the mercury intrusion porosimetry measurements, most pores were interconnected (i.e., the plates had fairly open-porous structures). In order to check the other liquid infiltrations, the HAp-46 plate was immersed in various kinds of liquids including polar and non-polar liquids (Table 2). All kinds of the liquids used here infiltrated inside the plate in a short time (within several tens seconds) with producing air bubbles, and the transparency of the HAp also increased. Surprisingly, the volume ratio of each liquid in the HAp was not influenced by the nature of liquid. This result might be due to relatively even dispersive (γ_{sv}^{d}, 34.2%) and polar (γ_{sv}^{p}, 65.8%) fractions of the surface tension of HAp (γ_{sv}, 46.7 mJ/m^2) [34]. The volume ratio of each liquid was around 50 vol.%, which is almost corresponded to the porosity (55%) determined from the mercury intrusion porosimetry measurement. Note that widely-used monomers (methyl methacrylate and ε-caprolactone) also could infiltrate inside the nanpores, and hence the mechanical or biodegradation properties would be controlled by polymerizing the monomer in the nanoporous HAp.

3.5. Protein adsorption and release

The adsorption and release of proteins were also investigated to examine the nanoporous HAp granules as reservoirs for drugs and growth factors. In this study, BSA and Cyt-c were used as model acidic and basic proteins, respectively. A number of studies have shown that protein adsorption on HAp is electrostatic in nature and that several different functional groups of protein and at least two possible adsorption sites on HAp surface may be involved [35,36]; That is, Ca^{2+} sites on *a* plane and PO_4^{3-} sites on *c* plane on a HAp

surface are believed to be protein binding sites. Acidic proteins including BSA bind preferentially onto *a* planes of HAp surfaces through Ca^{2+} bridging; whereas basic proteins including BSA preferentially bind onto *c* planes of HAp surfaces through PO_4^{3-} bridging.

As a control test, the HAp powders were prepared by grinding the HAp granules, and the adsorption profiles of BSA (Fig. 7b) and Cyt-c (Fig. 8b) were measured in the same procedure for the nanoporous granules. The protein adsorption on each HA powder ground was almost saturated within 1 day, which roughly corresponds to the protein adsorption behavior on nanoparticle-state HAp [37,38]. Although BSA is expected to bind onto the rod-shaped (and hence *a*-plane rich) HAp-320 powders more than other spherical HAp powders, the equilibrium adsorption amount of BSA was the smallest, which should be due to the smallest surface area of HAp-320 (see Supplementary Table S1). The Cyt-c adsorption onto rod-shaped (and hence *c*-plane poor) HAp-320 powders was smallest, as expected.

<Fig. 7>

<Fig. 8>

In the case of the nanoporous granules (Fig. 7a), the adsorption of BSA onto HAp-31 (pore size, 8.4 nm) or HAp-46 (pore size, 9.2 nm) granules delayed significantly compared with the powders, which should be because of the small pore size compared with the molecular size of BSA (5.0 nm × 7.0 nm × 7.0 nm [39]) and the long diffusion path (the diameter of HAp granules, around 1.5 mm). On the other hand, the degree of delay in Cyt-c adsorption onto each kind of granule was small (Fig. 8a), which should be due to smaller molecular size of Cyt-c (2.6 nm × 3.2 nm × 3.0 nm [39]) compared with BSA.

Finally, release profiles of each protein from the protein-adsorbed HAp granules were measured in PBS at 37˚C (Fig. 9). In the case of BSA release from the HAp-320 granules, the release was saturated within first 1 day, and BSA release was not observed after that, which may be due to the strong binding between BSA and rod-shaped HAp surfaces [40]. In the other cases, initial burst was observed within first 3 days, and sustained release was observed at least 4 weeks. It is known that release of medicine from HAp surface is controlled by ionic exchange on HA surface, degradation of HA carrier and diffusion of medicine [41]. Initial burst may be due to ionic exchange of protein molecules located on the outer surfaces of HA granules. The release rate of Cyt-c decreased with a decrease in the pore size, which supports that sustained release is caused by the penetration of PBS solution into the nanopores of HA granules and desorption of proteins from the pore surfaces. On the other hand, there is no significant difference among the release profiles of BSA from HAp-31, HAp-46 and HAp-73 granules. The reason is not clear at this moment but may be caused by the enlargement of pore size by dissolution of low-crystallinity HAp surface in the presence of BSA molecules [36]. Note that protein releasing from nanoparticle-state HAp is saturated within several tens of hours [35]. The long-term sustained release from the nanoporous HAp granules prepared here will be an important milestone for future bone regeneration systems based on HAp associated with human growth factor proteins.

<Fig. 9>

4. Conclusions

We clarified the preparation conditions of the novel method for preparing nanoporous

plates or granules consisting of low-crystallinity HAp nanoparticles by drying on an oil (flowable) substrate. The preparation method described here is simple and quick without template/binder molecules or high-temperature or high-pressure treatment. The nanoparticle-assembled transparent HAp showed low crystallinity with high surface area, which is largely different from the conventional transparent HAp sintered ceramics. We also clarified that several kinds of compounds could be infiltrated into the nanoporous HAp, and the proteins-adsorbed nanoporous HAp granules showed a long-term sustained release of proteins.

Acknowledgments

The SEM observations and XRD measurements were performed at the Institute of Dental Research, Osaka Dental University. The authors are grateful for the help offered by Dr. Syuji Fujii (Osaka Institute of Technology, Osaka, Japan) in facilitating access to helium pycnometry measurements. This study was supported in part by JSPS KAKENHI Grant Number 23792301.

AppendixA. Supplementarydata

Supplementary data associated with this article can be found, in the online version, at http://dx.doi.org/10.1016/j.apsusc…

REFERENCES

[1] H. Aoki, Science and medical application of hydroxyapatite, Ishiyaku EuroAmerica, St. Louis, 1991.

[2] K.L. Kilpadi, P.-L.Chang, S. L. Bellis, J. Biomed. Mater. Res. 57 (2001) 258–267.

[3] S. V. Dorozhkin J. Mater. Sci. 44 (2009) 2343–2387.

[4] M. Okada, T. Furuzono, Sci. Technol. Adv. Mater. 13 (2012) 064103.

[5] K. Gomi, B. Lowenberg, G. Shapiro, J. E. Davies, Biomaterials 14 (1993) 91–96.

[6] J. A. Gilles, D. L. Carnes, A. S. Windeler, J. Endodont. 20 (1994) 327–231.

[7] A. Bouladjine, A. Al-Kattan, P. Dufour, C. Drouet, Langmuir 25 (2009) 12256–12265.

[8] T. J. Webster, C. Ergun, R. H. Doremus, R. W. Siegel, R. Bizios, Biomaterials 22 (2001) 1327–1333.

[9] G. Balasundaram, M. Sato, T. J. Webster, Biomaterials 27 (2006) 2798–2805.

[10] W. Sun, C. Chu, J. Wang, H. Zhao, J. Mater. Sci. Mater. Med. 18 (2007) 677–683.

[11] J. Huang, S. M. Best, W. Bonfield, R. A. Brooks, N. Rushton, S. N. Jayasinghe, M. J. Edirisinghe, J. Mater. Sci. Mater. Med. 15 (2004) 441–445.

[12] M. R. Appleford, S. Oh, N. Oh, J. L. Ong, J. Biomed. Mater. Res. A 89 (2009) 1019–1027.

[13] J. Yao, W. Tjandra, Y. Z. Chen, K. C. Tam, J. Ma, B. Soh, J. Mater. Chem. 13 (2003) 3053–3057.

[14] F. Ye, H. Guo, H. Zhang, X. He, Acta Biomater. 6 (2010) 2212–2218.

[15] A. Raksujarit, K. Pengpat, G. Rujijanagul, T. Tunkasiri, Mater. Des. 31 (2010) 1658–1660.

[16] B. Arechabala, C. Coiffard, P. Rivalland, L.J.M. Coiffard, Y. De Roeck-Holtzhauer, J.

Appl. Toxicol. 19 (1999) 163–165.

[17] M. Okada, T. Furuzono, J. Colloid Interface Sci. 360 (2011) 457–462.

[18] K. Ioku, K. Yamamoto, K. Yanagisawa, N. Yamasaki, Phosphorus Res. Bull. 4 (1994) 65–70.

[19] K. Uematsu, M. Takagi, T. Honda, N. Uchida, K. Saito, J. Am. Ceram. Soc. 72 (1989) 1476–1478.

[20] H. Varma, S. P. Vijayan, S. S. Babu, J. Am. Ceram. Soc. 85 (2002) 493–495.

[21] K. Ioku, D. Kawagoe, H. Toya, H. Fujimori, S. Goto, K. Ishida, A. Mikuni, H. Mae, Trans. Mater. Res. Soc. Jpn. 27 (2002) 447–449.

[22] A. López-Macipe, J. Gómez-Morales, R. Rodríguez-Clemente, Adv. Mater. 10 (1998) 49–53.

[23] M.A. Martins, C. Santos, M.M. Almeida, M.E.V. Costa J. Colloid Interface Sci. 318 (2008) 210–216.

[24] M. T. Fulmer, I. C. Ison, C. R. Hankermayer, B. R. Constantz, J. Ross, Biomaterials 23 (2002) 751–755.

[25] M. S. Tirumkudulu, W. B. Russel, Langmuir 21 (2005) 4938–4948.

[26] W.B. Russel, N. Wu, W. Man, Langmuir 24 (2008) 1721–1730.

[27] H. Colina, S. Roux, Eur. Phys. J. E 1 (2000) 189–194.

[28] R. Chiu, T. Garino, M. Cima, J. Am. Ceram. Soc. 76 (1993) 2257–2264.

[29] R. Chiu, M. Cima, J. Am. Ceram. Soc. 76 (1993) 2769–2777.

[30] J. van de Lagemaat, K. D. Benkstein, A. J. Frank, J. Phys. Chem. B 105 (2001) 12433–12436.

[31] J. Wang, L.L. Shaw, Scr. Mater. 63 (2010) 593–596.

[32] Y. Yokogawa, Y. Shiotsu, F. Nagata, M. Watanabe, Trans. Mater. Res. Soc. Jpn. 29 (2004) 2375–2378.

[33] J.-Y. Hong, Y.J. Kim, H.-W. Lee, W.-K. Lee, J. S. Ko, H.-M. Kim, Biomaterials 24 (2003) 2977–2984.

[34] M.A. Lopes, F.J. Monteiro, J.D. Santos, A.P. Serro, B. Saramago, J. Biomed. Mater. Res. 45 (1999) 370–375.

[35] D.I. Hay, E.C. Moreno, J. Dent. Res. 58B (1979) 930–40.

[36] T. Kawasaki, S. Takahashi, K. Ikeda, Eur. J. Biochem. 152 (1985) 361–371.

[37] S. Dasgupta, A. Bandyopadhyay, S. Bose, Acta Biomateri. 5 (2009) 3112–3121.

[38] K. Kandori, A. Masunari, T. Ishikawa, Calcif. Tissue Int. 76 (2005) 194–206.

[39] M. Zhang, Y. Wu, X. Feng, X. He, L. Chen, Y. Zhang, J. Mater. Chem. 20 (2010) 5835–5842.

[40] T. Matsumoto, M. Okazaki, M. Inoue, S. Yamaguchi, T. Kusunose, T. Toyonaga, Y. Hamada, J. Takahashi, Biomaterials 25 (2004) 3807–3812.

[41] Y. Boonsongrit, H. Abe, K. Sato, M. Naito, M. Yoshimura, H. Ichikawa, Y. Fukumori, Mater. Sci. Eng. B 148 (2008) 162–165.

Table 1. Quantities employed to prepare HAp nanoparticles

		Abbreviation			
		HAp-31	HAp-46	HAp-73	HAp-320
Ca solution					
$(CH_3COO)_2Ca·H_2O$	(g)	5.97	———	———	———
$Ca(NO_3)_2·4H_2O$	(g)	———	8.00	8.00	8.00
NH_3 aq.[a)]	(mL)	5	5	5	5
Water	(mL)	800	800	800	800
PO_4 solution					
K_3PO_4	(g)	4.31	———	———	———
$(NH_4)_2HPO_4$	(g)	———	2.68	2.68	2.68
Water	(mL)	200	200	200	200
Temperature	(°C)	20	20	60	60
Addition rate of PO_4 solution		Within 5 sec	Within 5 sec	Within 5 sec	20 mL/h
Diameter[b)]	(nm)	31	46	73	320
S.D.[c)]	(nm)	5	18	31	118

[a)] 28% aqueous solution
[b)] Number-averaged diameter determined from SEM photographs
[c)] Standard deviation determined from SEM photographs

Table 2. Volumes of the liquids infiltrated in HAp-46 plates

Liquids	Volume %
Water	51 ± 10
Dodecane	56 ± 6
Dodecanol	54 ± 3
Methyl methacrylate	50 ± 9
ε-Caprolactone	57 ± 5

[a)] Calculated from the weight gain after infiltration of each liquid and the densities of each liquid and HAp-46 (2.85 g/cm^3).

FIGURE CAPTIONS

Figure 1. XRD patterns of HAp nanoparticles prepared by wet chemical processes under different conditions listed in Table 1: (a) HAp-31, (b) HAp-46, (c) HAp-73 and (d) HAp-320. The pattern (e) shows well-crystallized HAp calcined at 800˚C.

Figure 2. (a, b) Digital photographs of HAp-46 dispersions (2.0 wt.%; 5 mL) on oil (a: pure pentadecane; b: pure 1-dodecanol) substrates before drying, and (c) relationship between the composition of oil substrate and spreading area of HAp-46 dispersion on the oil substrate.

Figure 3. Digital photographs of HAp-nanoparticle-assembled (a–h) plates and (i–l) granules prepared by drying 2.0-wt.% HAp dispersions (a–h: 5 mL; i–l: 50 μL) on pure pentadecane substrates. The types of the nanoparticles: (a, e, i) HAp-31, (b, f, j) HAp-46, (c, g, k) HAp-73 and (d, h, l) HAp-320. The photographs (a–d) were taken before washing (and hence pentadecane was infiltrated in each plate) and the photographs (e–l) were taken after washing with ethanol followed by drying.

Figure 4. Visible light transmission of the HAp plates prepared by drying the HAp dispersions (2.0 wt.%; 5 mL) on pure pentadecane substrates. The measurements were conducted with the plates (a) after washing with ethanol followed by drying and (b) after re-immersed in pentadecane.

Figure 5. SEM photographs of the surfaces of HAp plates prepared by drying the HAp dispersions (2.0 wt.%; 5 mL) on pure pentadecane substrates. The types of nanoparticles: (a) HAp-31, (b) HAp-46, (c) HAp-73 and (d) HAp-320. The insets show magnified images.

Figure 6. Pore-size distributions in HAp plates prepared by drying the HAp dispersions (2.0

wt.%; 5 mL) on pure pentadecane substrates

Figure 7. Absorption profiles of BSA (initial concentration, 200 μg/mL in PBS; total volume, 0.5 mL) on 10 mg of (a) 1.5 mm sized HAp granules and (b) HAp powders. The HAp granules were prepared by drying the HAp dispersions (2.0 wt.%; 50 μL) on pure pentadecane substrates, and the HAp powders were prepared by grinding the HAp granules with using a mortar and pestle.

Figure 8. Absorption profiles of Cyt-c (initial concentration, 200 μg/mL in PBS; total volume, 0.5 mL) on 10 mg of (a) 1.5 mm sized HAp granules and (b) HAp powders. The HAp granules were prepared by drying the HAp dispersions (2.0 wt.%; 50 μL) on pure pentadecane substrates, and the HAp powders were prepared by grinding the HAp granules with using a mortar and pestle.

Figure 9. Release profiles of (a) BSA and (b) Cyt-c from the protein-adsorbed HAp granules in PBS at 37˚C. The protein-adsorbed HAp granules were prepared by immersing 10 mg of HAp granules in each protein solution (200 μg/mL; 0.5 mL) at room temperature for 10 days. The percentage of protein released were calculated against the total amount of protein adsorbed.

Fig. 1

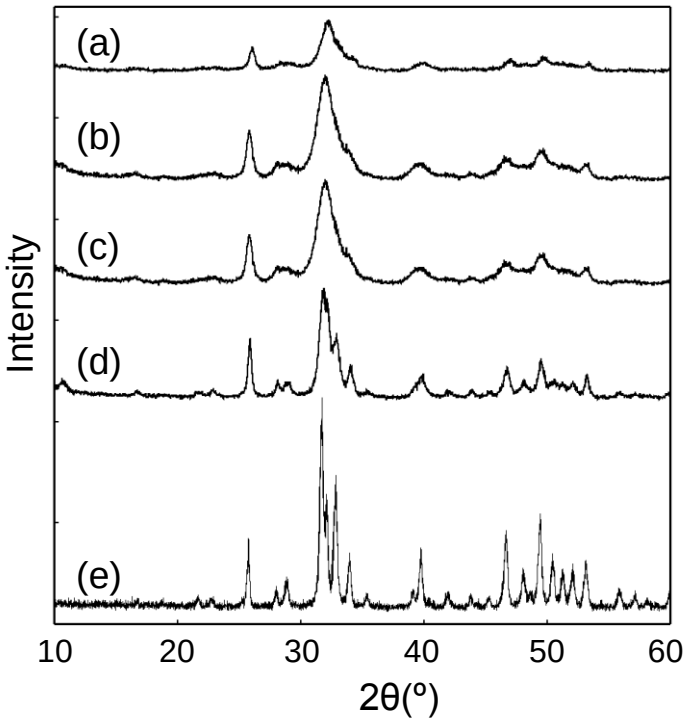

Figure 1. XRD patterns of HAp nanoparticles prepared by wet chemical processes under different conditions listed in Table 1: (a) HAp-31, (b) HAp-46, (c) HAp-73 and (d) HAp-320. The pattern (e) shows well-crystallized HAp calcined at 800˚C.

Fig. 2

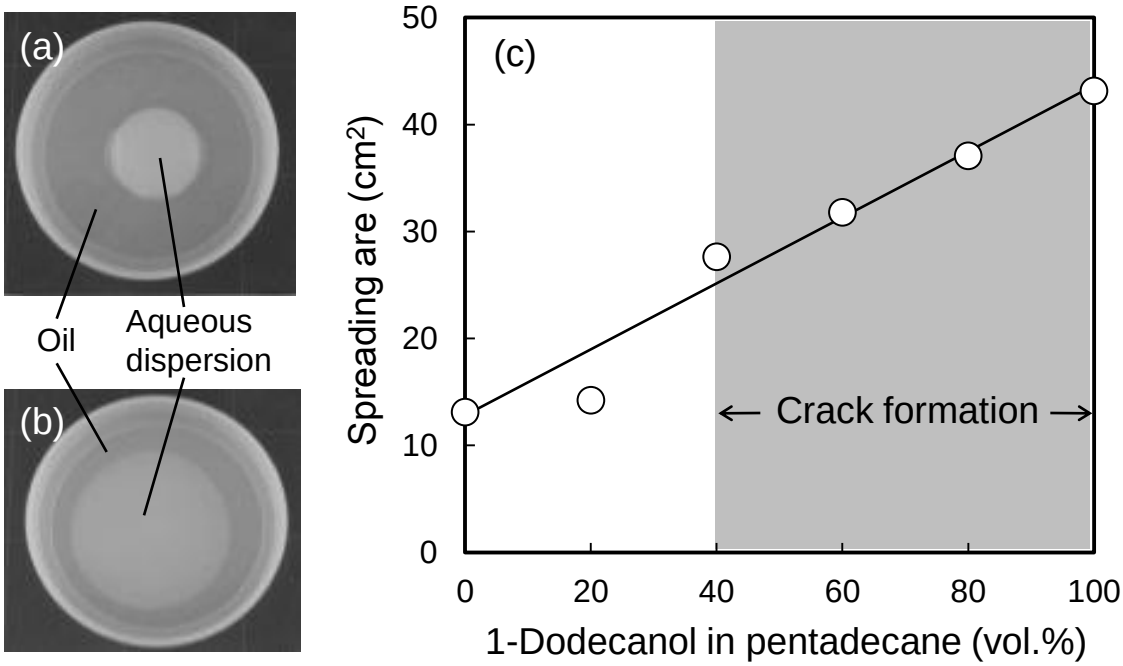

Figure 2. (a, b) Digital photographs of HAp-46 dispersions (2.0 wt.%; 5 mL) on oil (a: pure pentadecane; b: pure 1-dodecanol) substrates before drying, and (c) relationship between the composition of oil substrate and spreading area of HAp-46 dispersion on the oil substrate.

Fig. 3

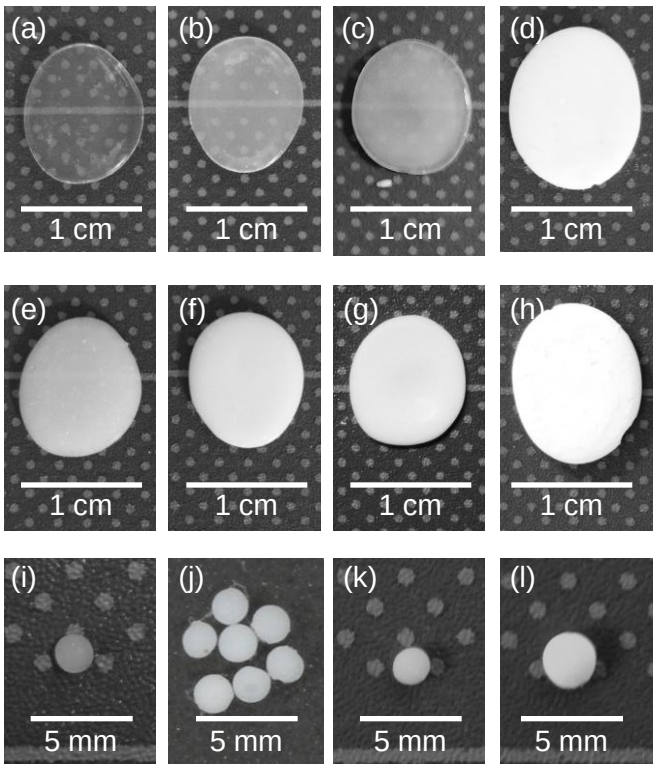

Figure 3. Digital photographs of HAp-nanoparticle-assembled (a–h) plates and (i–l) granules prepared by drying 2.0-wt.% HAp dispersions (a–h: 5 mL; i–l: 50 μL) on pure pentadecane substrates. The types of the nanoparticles: (a, e, i) HAp-31, (b, f, j) HAp-46, (c, g, k) HAp-73 and (d, h, l) HAp-320. The photographs (a–d) were taken before washing (and hence pentadecane was infiltrated in each plate) and the photographs (e–l) were taken after washing with ethanol followed by drying.

Fig. 4

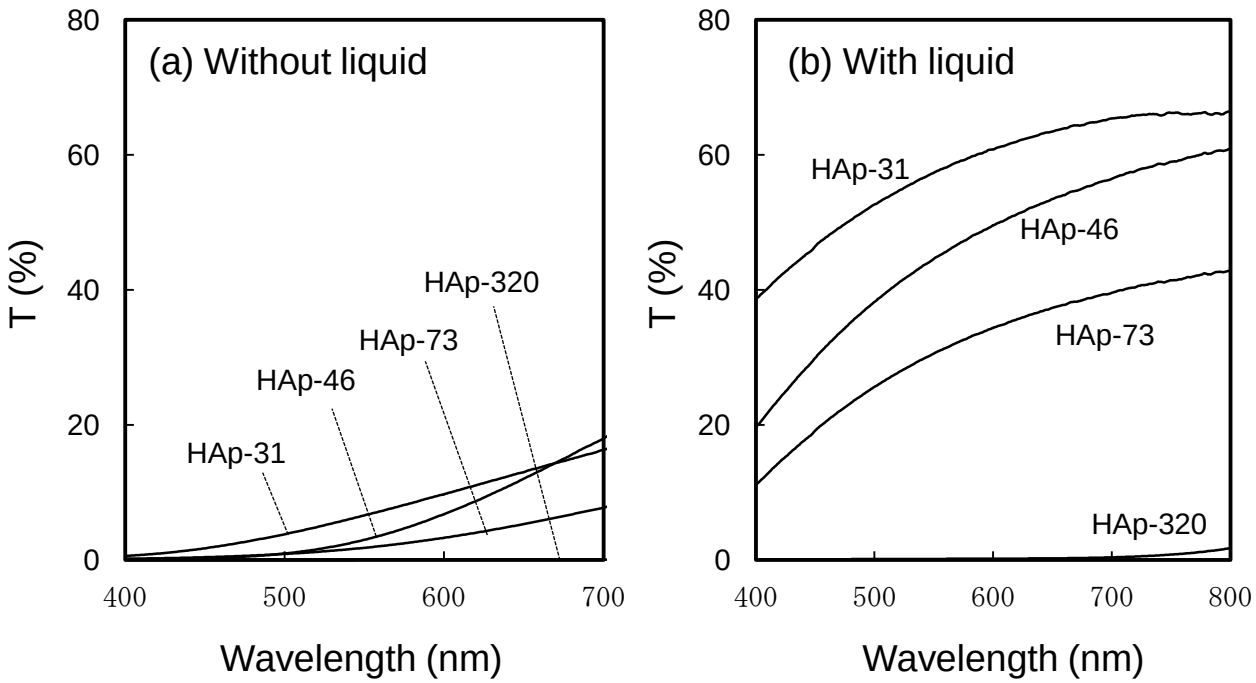

Figure 4. Visible light transmission of the HAp plates prepared by drying the HAp dispersions (2.0 wt.%; 5 mL) on pure pentadecane substrates. The measurements were conducted with the plates (a) after washing with ethanol followed by drying and (b) after re-immersed in pentadecane.

Fig. 5

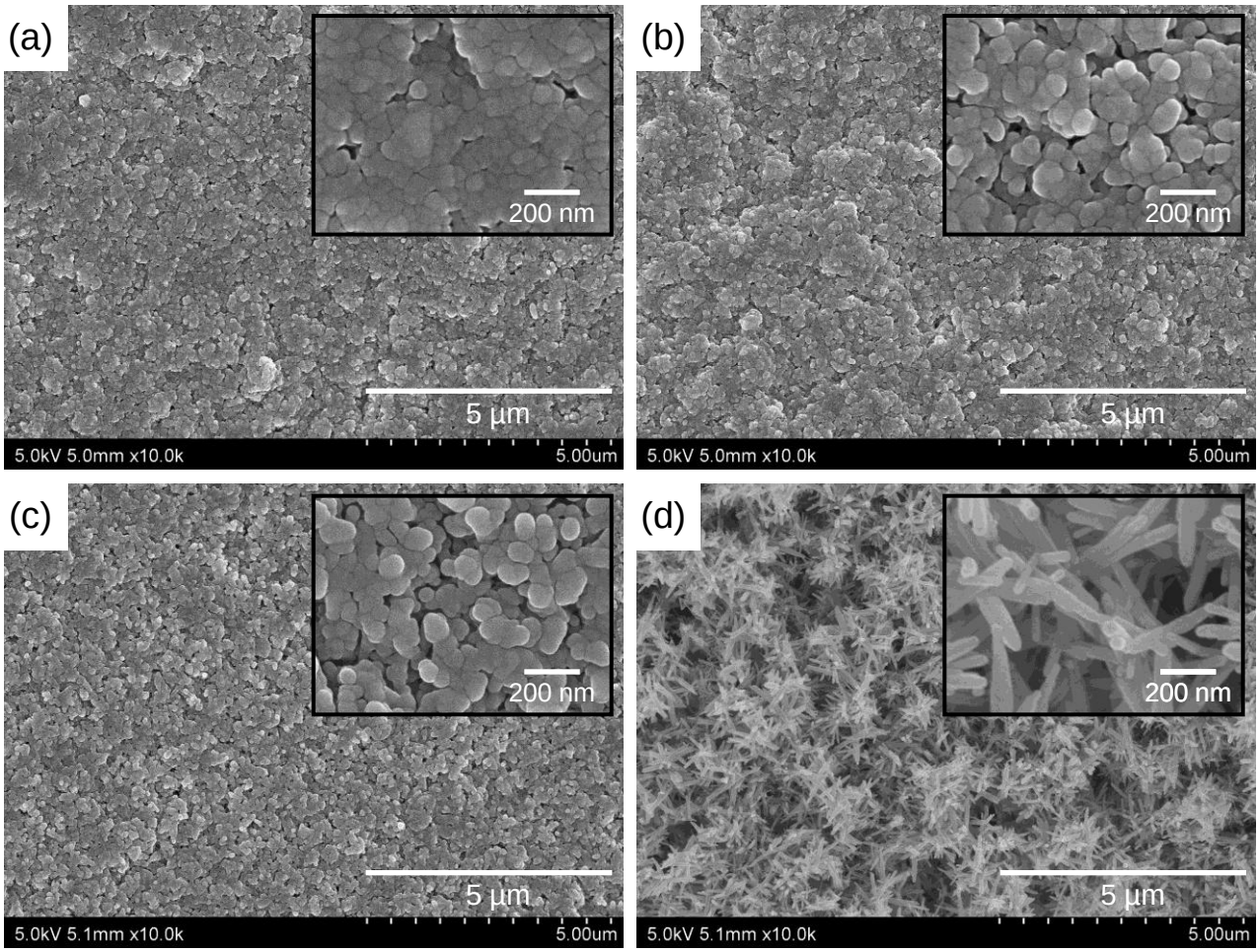

Figure 5. SEM photographs of the surfaces of HAp plates prepared by drying the HAp dispersions (2.0 wt.%; 5 mL) on pure pentadecane substrates. The types of nanoparticles: (a) HAp-31, (b) HAp-46, (c) HAp-73 and (d) HAp-320. The insets show magnified images.

Fig. 6

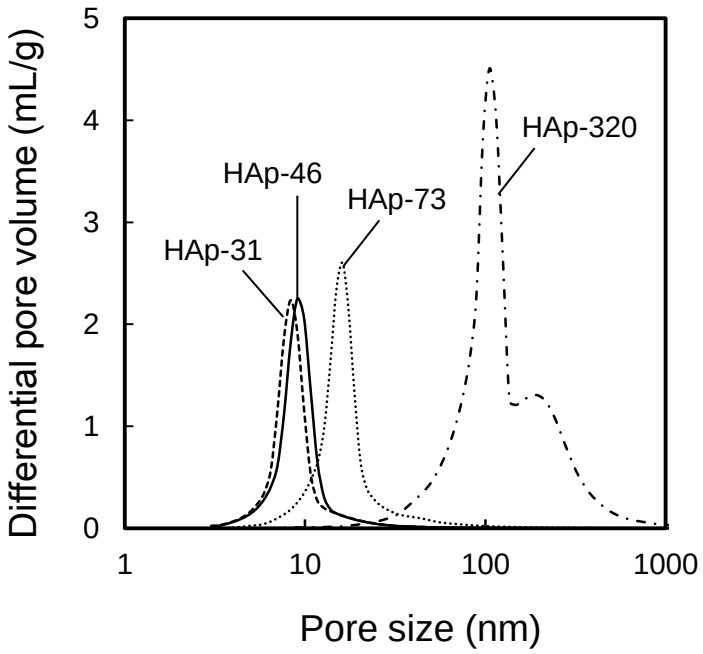

Figure 6. Pore-size distributions in HAp plates prepared by drying the HAp dispersions (2.0 wt.%; 5 mL) on pure pentadecane substrates

Fig. 7

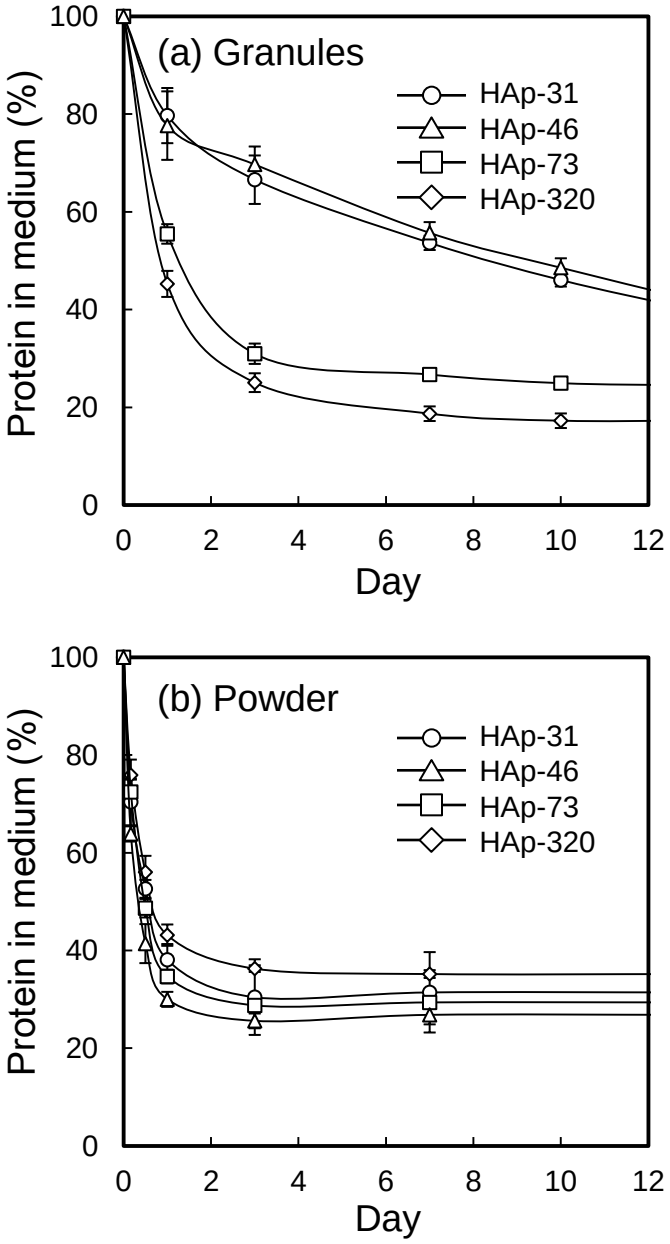

Figure 7. Absorption profiles of BSA (initial concentration, 200 μg/mL in PBS; total volume, 0.5 mL) on 10 mg of (a) 1.5 mm sized HAp granules and (b) HAp powders. The HAp granules were prepared by drying the HAp dispersions (2.0 wt.%; 50 μL) on pure pentadecane substrates, and the HAp powders were prepared by grinding the HAp granules with using a mortar and pestle.

Fig. 8

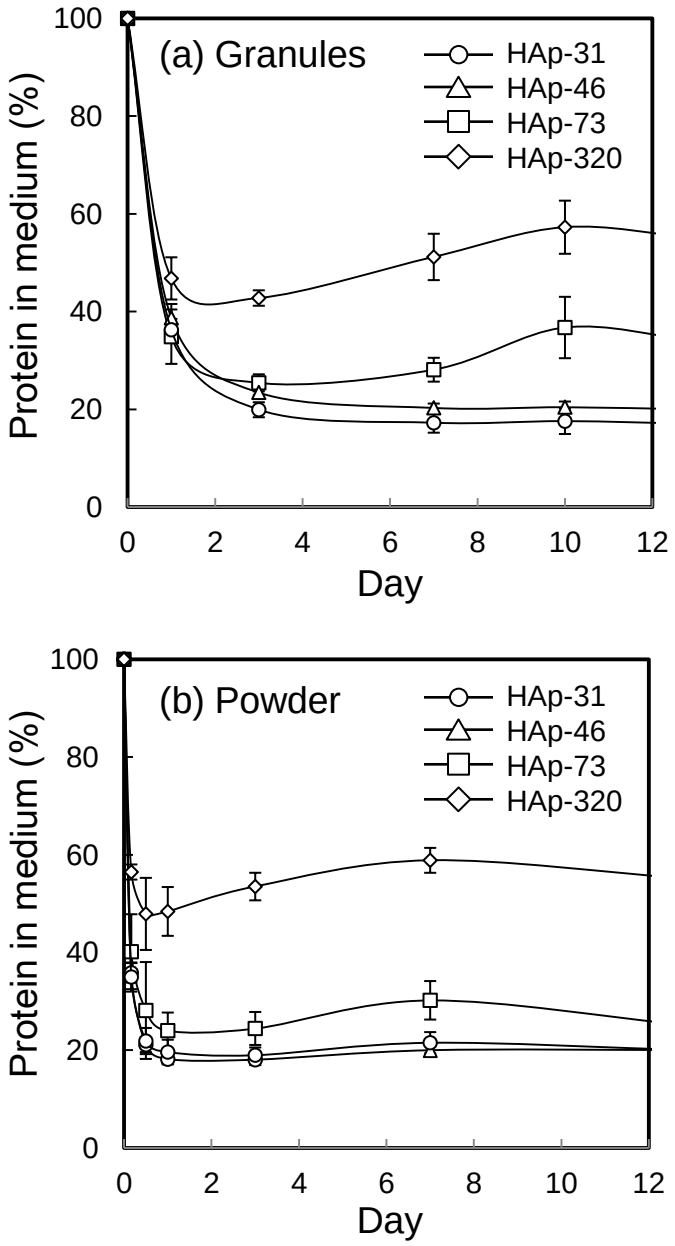

Figure 8. Absorption profiles of Cyt-c (initial concentration, 200 μg/mL in PBS; total volume, 0.5 mL) on 10 mg of (a) 1.5 mm sized HAp granules and (b) HAp powders. The HAp granules were prepared by drying the HAp dispersions (2.0 wt.%; 50 μL) on pure pentadecane substrates, and the HAp powders were prepared by grinding the HAp granules with using a mortar and pestle.

Fig. 9

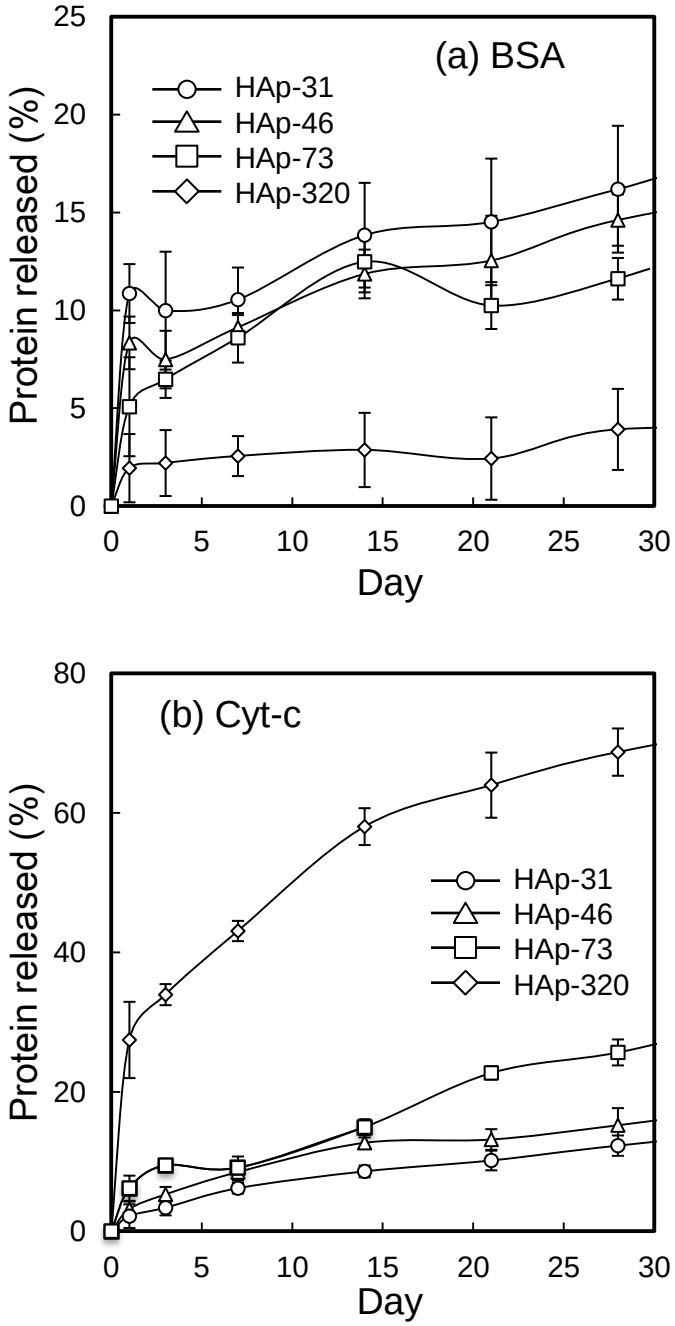

Figure 9. Release profiles of (a) BSA and (b) Cyt-c from the protein-adsorbed HAp granules in PBS at 37˚C. The protein-adsorbed HAp granules were prepared by immersing 10 mg of HAp granules in each protein solution (200 μg/mL; 0.5 mL) at room temperature for 10 days. The percentage of protein released were calculated against the total amount of protein adsorbed.

Supplementary materials

Click here to download Supplementary materials: 6-Supplementary_data.pdf